Investigating the upper and lower energy cutoffs of EMIC-wave driven precipitation events

A. T. Hendry[*1], *C. J. Rodger*[1], *B. R. Carson*[1], *and M. A. Clilverd*[2]

[1]Department of Physics, University of Otago, P.O. Box 56, Dunedin, New Zealand (ahendry@physics.otago.ac.nz, crodger@physics.otago.ac.nz, no email)

[2]British Antarctic Survey, Cambridge, United Kingdom (macl@bas.ac.uk)

Abstract

For some time theoretical modelling has shown that electromagnetic ion cyclotron (EMIC) waves should play an important role in the loss of relativistic electrons from the radiation belts, through precipitation of the electrons into the polar ionosphere. However, there are limited direct experimental observations of relativistic electron precipitation occurring, despite the indirect evidence for its importance. We report on a study that determines the typical flux impacting the ionospheric D-region during EMIC-driven precipitation events, and the effect this has on ionospheric conditions. We examine a very large set of EMIC-driven electron precipitation events detected using data from the Polar-orbiting Operational Environmental Satellite (POES) constellation [1] and determine the typical precipitating electron and proton fluxes and associated energy cutoffs.

1. Introduction

Electromagnetic ion cyclotron (EMIC) waves have long been known to play a role in electron loss processes from the radiation belts, though the extent of their involvement has been a matter of some debate. EMIC waves are able to interact with protons with energies of tens of keV through cyclotron resonance [2]. The same waves may also resonant with relativistic electrons through "anomalous" cyclotron resonance [3]. The resonance conditions in this case exclude low-energy electrons from interacting with the wave, but there is uncertainty concerning the lower energy cutoff. Studies present conflicting results as to the energy range of the lower energy cutoff, with some suggesting cutoffs as low as a few hundred keV [e.g. 4, 5] while others showed cutoff energies up to ~ 10 MeV [e.g. 6–8]. In order to be an efficient driver of electron precipitation, EMIC waves must be capable of interacting with electrons of energies less than $\sim 1-2$ MeV. Thus a cutoff of a few hundred keV would suggest EMIC waves could be very important drivers of radiation belt loss (and atmospheric coupling), while a ~ 10 MeV cutoff would suggest it was unimportant for the fluxes that tend to exist in the radiation belts.

1.1 Instrumentation

The Polar-orbiting Operational Environmental Satellite (POES) constellation is a set of satellites in sun-synchronous orbit around the earth. Since the launch of the NOAA-15 satellite in 1998 each POES satellite carries a Medium Energy Proton and Electron Detector (MEPED), which is used for monitoring particles fluxes within the radiation belts. Each MEPED instrument consists of two pairs of directional telescopes, with one of each pair measuring electrons and the other measuring protons. The telecopes are aligned such that one pair points antiparallel to the satellites velocity direction (90°) and the other points in a direction radially outwards from the centre of the earth. This means that at higher L-shells ($\sim> 2$) the 0°detector will sample the bounce loss cone flux, while the 90°detector will sample the trapped particle flux [9]. Each telescope pair has an electron telescope and a proton telescope, which are further divided into energy channels. The proton telescopes each have six energy channels, which nominally measure proton flux from > 30 keV to > 6900 keV. The electron telescopes each have three energy channels, which nominally measure electron flux from > 30 keV to > 300 keV. For more information on these channels see the technical paper by Evans and Greer [10].

1.2 EMIC Event Database

Cyclotron resonance can pitch angle scatter particles into the bounce loss cone, resulting in the precipitation of the particles into the ionosphere [11]. This combination of low-energy proton precipitation and relativistic electron precipitation forms a signature that can be used to search for EMIC-waves in radiation belt particle flux data. Sandanger et al. [12] showed that this signature is present in data from the POES MEPED flux data, seen as simultaneous spikes in the 0° P1 channel (30-80 keV protons) and the 0° P6 channel (>800 keV electrons), both of which sample the bounce loss cone flux. Carson et al. [1] used the POES MEPED data and this signature to generate a database of 2331 EMIC-wave driven REP events during the period from 1998-2010. The events in this database occur predominantly in the outer radiation belt (3<L<7), with most occurring slightly outside the plasmapause. The majority of the events were found to occur in the dusk and night MLT sectors.

978-1-4673-5225-3/14/$31.00

2. POES Derived Particle Energy Spectra

To determine the effect that EMIC-wave driven REP has on the ionosphere, it is necessary to quantify the electron flux that reaches the ionosphere during the events. The Carson et al. [1] events were defined based on spikes in the POES flux data, so we use this data to investigate the precipitating flux. It has long been known that the POES MEPED instruments suffer from cross contamination between the electron and proton channels [e.g. 12]. Modelling by Yando et al. [13] provided energy dependent geometric factors $G(E)$ for each of the MEPED directional flux channels, which quantify how each channel responds to electron and proton flux. Using these geometric factors, it is possible to convert an electron or proton energy spectra into a "apparent flux" value for each channel, which represents the flux that would be recorded by the channel in response to that spectra. By combining the apparent flux response to both protons and electrons, we can model how the POES MEPED channels respond to a particular radiation belt state.

As mentioned in Section 1, EMIC waves can pitch angle scatter both energetic protons and relativistic electrons. The presence of energetic protons means that there is likely to be significant proton contamination in the electron channels during EMIC-driven REP [10]. In order to account for this contamination we must fit both electron and proton spectra to the data. Electrons with energies below the minimum electron resonance energy for a given EMIC wave will not be pitch-angle scattered, nor will protons above the maximum proton resonance energy. To model this, we use energy spectra with hard cutoffs at these points. For the electron flux distribution $j_e(E)$ we use an e-folding distribution with e-folding energy κ_e, lower energy cutoff E_{lc}, and amplitude A_e. For the proton flux distribution $j_p(E)$ we use a power-law distribution with power gradient κ_p, upper energy cutoff E_{uc}, and amplitude A_p. These distributions are outlined in equation (1). When combined with the Yando et al. [13] geometric factors, as shown in equation (2), we can determine the apparent flux contributed to each channel by each spectrum. Using the E1 channel as an example, we can combining the proton and electron flux contributions as in equation (3) to get the apparent flux for each channel. The 10 MeV limit in equations (2) and (3) arises from the limit on the geometric factors from Yando et al. [13].

$$j_e(E) = \begin{cases} E < E_{lc} & : 0 \\ E \geq E_{lc} & : A_e e^{-E/\kappa} \end{cases} \qquad j_p(E) = \begin{cases} E < E_{uc} & : A_p E^{\kappa_p} \\ E \geq E_{uc} & : 0 \end{cases} \tag{1}$$

$$C = \sum_{E\,=\,0\text{ keV}}^{10\text{ MeV}} j(E)G(E) \tag{2}$$

$$C_{\mathrm{E1}} = \sum_{E\,=\,0\text{ keV}}^{10\text{ MeV}} j_e(E)G_{\mathrm{E1}_e}(E) + \sum_{E\,=\,0\text{ keV}}^{10\text{ MeV}} j_p(E)G_{\mathrm{E1}_p}(E) \tag{3}$$

2.1 Modelling the POES Flux Response

For each event in the Carson et al. [1] database, we attempt to reproduce the POES measured flux with an apparent flux generated from an electron spectrum and a proton spectrum. We are interested in the bounce loss-cone flux, so we look at the nine 0° channels from the POES MEPED instrument. The apparent flux for each of these channels has an electron contributed component and a proton contributed component, the ratio of which is determined by the particular spectra and the geometric factors of the channel.

We use a combination of brute-force and iterative methods to determine the best electron and proton spectra fitted to represent the measured flux for a given event. We filter the parameter space to only include spectra that can possibly represent the target flux values; for instance, we exclude spectra that generate flux in channels where the measured flux is zero. We use the filtered fitted spectra to calculate the maximum and minimum electron and proton flux contributions for each channel, and exclude spectra that produce fluxes outside this range. We repeat this process until the set of possible fitted spectra stabilises. We then search the remaining fitted spectra to find the combination of electron and proton spectra that best represents the measured flux. We repeat this process for each event in the Carson et al. [1] database.

2.2 Results

Of the 2331 events in the Carson et al. [1] database, our fitting process was able to fit 1611 of them (roughly 70%); we discuss the reasons for the non-fitted events in the next section. The electron e-folding energies and lower energy cutoffs of the fitted events are shown in Figure 1. The electron lower energy cutoff has two peaks - one around 30 keV, and the other at around 600 keV. The first peak is caused by electron flux in the lower energy electron channels E1 and E2 (which nominally measure > 30 and > 100 keV electron flux respectively) which cannot be explained by proton contamination alone. In these instances, the fitting process has to push the electron cutoff energy down to account for the low energy electron flux. The second peak starts at around 400 keV and extends to about 1.3 MeV. The electron e-folding energy distribution peaks around 200 keV with a long tail that stretches out to ~ 2.5 MeV.

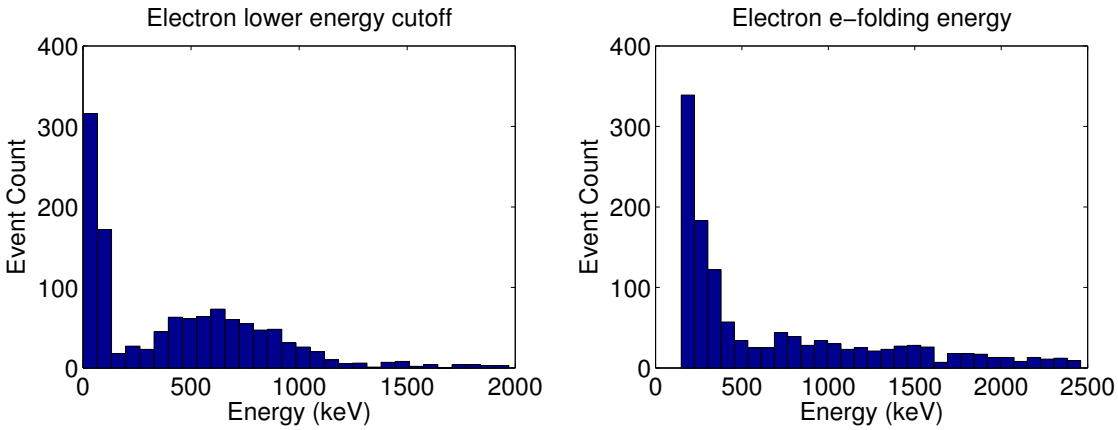

Figure 1: (left) The fitted electron lower energy cutoff histogram for the Carson et al. [1] EMIC-driven REP events. The main occurence peak occurs around 400 keV, with a secondary peak at the low end of the energy range. (right) The electron e-folding energy histogram for the same events. The main peak occurs around 200 keV.

3. Discussion

A significant number of the events from the Carson et al. [1] database could not be fit by our fitting process. A small number ($\sim$ 50) of these failures were due to false flags from the Carson et al. [1] detection algorithm; the POES MEPED flux values for these events clearly do not represent EMIC-wave driven REP events. However we believe that the majority of the non-fitting events are due to the failure of the assumption that the electron and proton spectra can be fit by e-folding and power-law distributions respectively. While this assumption is appropriate in the majority of cases, it may no longer hold if background flux significantly changes the energy distributions of the electrons or protons. Substorms are a known driver of EMIC-wave activity [e.g. 14], but are also significant source of electron and proton precipitating fluxes. Contamination of the EMIC wave driven precipitation with essentially independent substorm driven precipitation would likely perturb the energy distributions enough to cause the fitting to fail; we believe that is what is happening in the majority of those cases.

In some cases, low energy electron flux, for instance from substorms, may contaminate the EMIC driven REP flux, but not enough to cause the fitting to fail. In this case, the presence of substorm flux would be seen as a large increase in electron flux in the E1 and E2 channels. This in turn would drive down the electron lower energy cutoff of the fit in order to account for these lower energy electrons. We believe this is the cause of the low energy peak in the electron cutoff energy shown in Figure 1. If we remove events with an electron cutoff < 150 keV (~ 150 events) we are left with the distributions shown in Figure 2. Removing these events reduces the upper tail of the electron e-folding energy to about 600 keV.

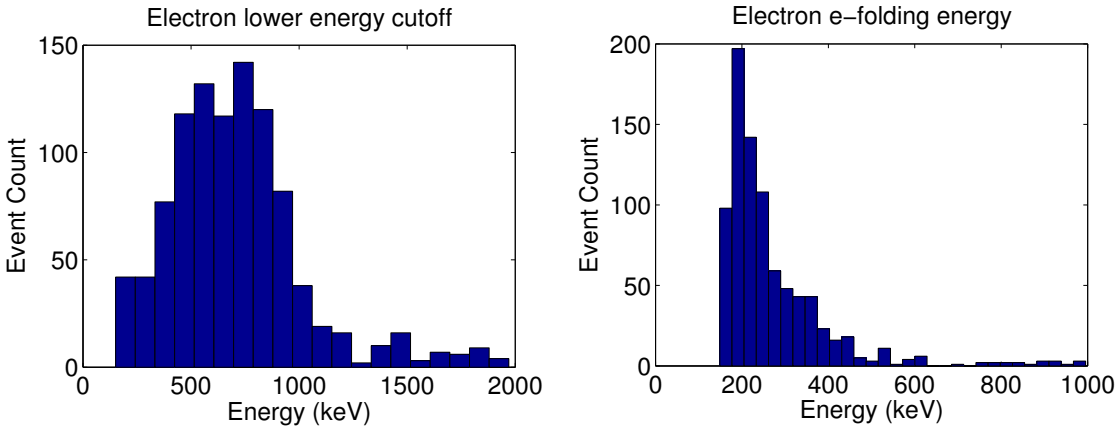

Figure 2: The same histograms as in Figure 1 with events with low energy electron contamination removed.

4. Conclusions

These results show that EMIC-wave interactions with radiation belt electrons may occur at energies as low as 400keV, with the majority of events having a lower electron cutoff < 1 MeV. These low cutoff energies allow EMIC-waves to resonate with the electrons that make up the bulk of the outer radiation belt. This suggests that EMIC-waves are a significant driver of electron losses from the radiation belts.

References

[1] B. R. Carson, C. J. Rodger, and M. A. Clilverd, "POES satellite observations of EMIC-wave driven relativistic electron precipitation during 1998–2010," *Journal of Geophysical Research: Space Physics*, vol. 118, no. 1, pp. 232–243, 2013. [Online]. Available: http://dx.doi.org/10.1029/2012JA017998

[2] V. K. Jordanova, M. Spasojevic, and M. F. Thomsen, "Modeling the electromagnetic ion cyclotron wave-induced formation of detached subauroral proton arcs," *Journal of Geophysical Research: Space Physics*, vol. 112, no. A8, pp. n/a–n/a, 2007. [Online]. Available: http://dx.doi.org/10.1029/2006JA012215

[3] B. T. Tsurutani and G. S. Lakhina, "Some basic concepts of wave-particle interactions in collisionless plasmas," *Reviews of Geophysics*, vol. 35, no. 4, pp. 491–501, 1997. [Online]. Available: http://dx.doi.org/10.1029/97RG02200

[4] A. Ukhorskiy, Y. Shprits, B. Anderson, K. Takahashi, and R. Thorne, "Rapid scattering of radiation belt electrons by storm-time EMIC waves," *Geophysical Research Letters*, vol. 37, no. 9, p. L09101, 2010.

[5] Y. Omura and Q. Zhao, "Nonlinear pitch angle scattering of relativistic electrons by EMIC waves in the inner magnetosphere," *Journal of Geophysical Research: Space Physics (1978–2012)*, vol. 117, no. A8, 2012.

[6] N. P. Meredith, R. M. Thorne, R. B. Horne, D. Summers, B. J. Fraser, and R. R. Anderson, "Statistical analysis of relativistic electron energies for cyclotron resonance with EMIC waves observed on CRRES," *Journal of Geophysical Research: Space Physics*, vol. 108, no. A6, pp. n/a–n/a, 2003. [Online]. Available: http://dx.doi.org/10.1029/2002JA009700

[7] R. Millan, R. Lin, D. Smith, and M. McCarthy, "Observation of relativistic electron precipitation during a rapid decrease of trapped relativistic electron flux," *Geophysical research letters*, vol. 34, no. 10, 2007.

[8] I. Silin, I. Mann, R. Sydora, D. Summers, and R. Mace, "Warm plasma effects on electromagnetic ion cyclotron wave MeV electron interactions in the magnetosphere," *Journal of Geophysical Research: Space Physics (1978–2012)*, vol. 116, no. A5, 2011.

[9] C. J. Rodger, B. R. Carson, S. A. Cummer, R. J. Gamble, M. A. Clilverd, J. C. Green, J.-A. Sauvaud, M. Parrot, and J.-J. Berthelier, "Contrasting the efficiency of radiation belt losses caused by ducted and nonducted whistler-mode waves from ground-based transmitters," *Journal of Geophysical Research: Space Physics (1978–2012)*, vol. 115, no. A12, 2010.

[10] D. S. Evans and M. S. Greer, *Polar Orbiting Environmental Satellite Space Environment Monitor-2: Instrument Description and Archive Data Documentation*. US Department of Commerce, National Oceanic and Atmospheric Administration, Oceanic and Atmospheric Research Laboratories, Space Environment Center, 2000.

[11] D. Summers and R. M. Thorne, "Relativistic electron pitch-angle scattering by electromagnetic ion cyclotron waves during geomagnetic storms," *Journal of Geophysical Research: Space Physics*, vol. 108, no. A4, pp. n/a–n/a, 2003. [Online]. Available: http://dx.doi.org/10.1029/2002JA009489

[12] M. Sandanger, F. Søraas, M. Sørbø, K. Aarsnes, K. Oksavik, and D. Evans, "Relativistic electron losses related to EMIC waves during CIR and CME storms," *Journal of Atmospheric and Solar-Terrestrial Physics*, vol. 71, no. 10–11, pp. 1126 – 1144, 2009, high Speed Solar Wind Streams and Geospace Interactions High Speed Solar Wind Streams and Geospace Interactions. [Online]. Available: http://www.sciencedirect.com/science/article/pii/S1364682608001946

[13] K. Yando, R. M. Millan, J. C. Green, and D. S. Evans, "A Monte Carlo simulation of the NOAA POES Medium Energy Proton and Electron Detector instrument," *Journal of Geophysical Research: Space Physics*, vol. 116, no. A10, pp. n/a–n/a, 2011. [Online]. Available: http://dx.doi.org/10.1029/2011JA016671

[14] M. Usanova, I. Mann, J. Bortnik, L. Shao, and V. Angelopoulos, "THEMIS observations of electromagnetic ion cyclotron wave occurrence: Dependence on AE, SYMH, and solar wind dynamic pressure," *Journal of Geophysical Research: Space Physics (1978–2012)*, vol. 117, no. A10, 2012.